Low-Frequency Basin Modes in a Two-Layer Quasigeostrophic Model in the Presence of a Mean Gyre Flow*

MAHDI BEN JELLOUL

Woods Hole Oceanographic Institution, Woods Hole, Massachusetts

THIERRY HUCK

Laboratoire de Physique des Océans, CNRS, Brest, France

(Manuscript received 15 December 2004, in final form 7 April 2005)

ABSTRACT

The spectrum of baroclinic basin modes is investigated in a two-layer wind-driven quasigeostrophic model through weakly nonlinear multiple time-scale expansion in the Burger number. The baroclinic basin modes are mainly advected by a barotropic steady Sverdrup flow. Emphasis is given to the regularizing influence of dispersion rather than to dissipation. In the inviscid large-scale limit, that is, for basin scale considerably larger than the Rossby radius of deformation, all of the basin modes are neutral. Their typology is then numerically examined (with some necessary dissipation), and their frequency and spatial properties are discussed. Three types of modes arise for some wind forcing strong enough to produce a recirculating gyre with closed geostrophic contours: the classical Rossby basin modes deformed by the mean flow (shadow modes), stationary modes, and recirculating pool modes, the two latter being trapped in the closed-contours pool. Focus is made here on the recirculating modes that could have very low frequencies for moderate recirculating gyres. Strong gyres lead to higher frequencies, and recirculating modes resonate with deformed Rossby basin modes.

1. Introduction

Analysis of historical oceanic data (Kushnir 1994; Mann et al. 1998, among many others) provides evidence of interannual to interdecadal variability, also found in coupled (Delworth et al. 1993) and ocean (Greatbatch and Zhang 1995; Colin de Verdière and Huck 1999; Delworth and Greatbatch 2000) general circulation models. Baroclinic Rossby basin modes suggest a possible explanation for these variability signals; they are westward-propagating Rossby waves reinitiated at the eastern boundary through rapid Kelvin wave adjustment (LaCasce 2000) or nonresonant inertia–gravity wave response (Primeau 2002). Global observations (Chelton and Schlax 1996) have also revealed in tropical regions a more coherent signal and anomalously faster propagation than in the northern part of the subtropical gyre; see the introduction in Spydell and Cessi (2003) and references therein for a thorough review.

In the inviscid case, all basin modes are neutral, whatever their spatial scale, in the absence of a mean circulation. In the context of a reduced-gravity one-layer model, Cessi and Primeau (2001) argued that stochastic (white noise) atmospheric forcing equally excites basin modes, but also that only the low-frequency part of the spectrum emerges because of dissipation: the low-frequency modes are, indeed, the large-scale ones and are thus less dissipated and more resonant. In the presence of a mean flow, the dissipative selection mechanism may not survive. Indeed, the nonlinear interactions could promote a growing mode fed by the mean flow (Ben Jelloul and Huck 2003).

More realistic ocean models must include, at least, two active layers. Here, we will treat the simple academic case of a quasigeostrophic two-layer ocean forced by a time-independent wind stress in a closed

* Woods Hole Oceanographic Institution Contribution Number 10999.

Corresponding author address: Thierry Huck, Laboratoire de Physique des Océans, Université de Bretagne Occidentale, UFR Sciences F.308, 6 avenue Le Gorgeu, CS 93837, 29238 Brest Cedex 3, France.
E-mail: thuck@univ-brest.fr

basin (section 2). Some recent studies on the ocean adjustment to wind forcing via baroclinic Rossby wave have shown the advecting role of the mean flow (Sirven and Frankignoul 2000; Dewar and Huang 2001). Spydell and Cessi (2003, SC03 hereinafter) recently examined the baroclinic eigenmodes in a two-layer configuration where the barotropic mode is decoupled; they analytically considered an approximated inviscid problem and numerically solved the forced–dissipated case. They identified oscillatory basin modes in the shadow region (hence named shadow modes) as well as pool modes in the case of closed geostrophic contours. They did not retain the dispersion terms in their model equations and found baroclinic mode damping independent of friction (Cessi and Louazel 2001). As we shall see hereinafter, this is not the case whenever dispersion is conserved, which allows an alternative adjustment to boundary conditions.

Low values of the Burger number, defined as the squared ratio of the Rossby radius of deformation to the basin length, are typical of basinwide oceanic circulations. The use of the Burger number as a small parameter for a weak nonlinear multiple-time-scale expansion allowed us to separate the Sverdrup flow from the barotropic basin modes (section 3) and baroclinic modes (section 4). Baroclinic modes consist of resonant Rossby waves whose propagation is influenced by the steady barotropic flow. Different types of modes can arise depending on the relative strength of the barotropic mean flow advection and Rossby waves velocity: they are numerically found for various regimes in the parameter space (section 5). Differences with SC03 resulting from the relative role of the dissipation and dispersion to the type of mode will be outlined throughout the paper. Last, we will discuss our results, draw conclusions, and suggest new developments in the way these investigations could be pursued to study nonlinear mode selection by the mean flow (section 6).

2. System setup

a. Quasigeostrophic dynamics

The quasigeostrophic (QG) potential vorticity equations for two active layers read in terms of the upper ($i = 1$) and lower ($i = 2$) layers streamfunctions ψ_i ($\mathrm{m^2\,s^{-1}}$):

$$[\partial_t + J(\psi_1, \cdot)][\nabla^2\psi_1 - F_1(\psi_1 - \psi_2) + \beta y] = \frac{f_0}{H_1} W_E + \kappa\nabla^2[\nabla^2\psi_1 - F_1(\psi_1 - \psi_2)] \quad \text{and} \tag{1a}$$

$$[\partial_t + J(\psi_2, \cdot)][\nabla^2\psi_2 - F_2(\psi_2 - \psi_1) + \beta y] = \kappa\nabla^2[\nabla^2\psi_2 - F_2(\psi_2 - \psi_1)] - \lambda\nabla^2\psi_2, \tag{1b}$$

where

$$F_i = \frac{f_0^2}{g' H_i}, \quad g' = \frac{\rho_2 - \rho_1}{\rho_0} g, \tag{2}$$

g is the gravity acceleration, H_i (ρ_i) are the layer thicknesses (densities), ρ_0 is the seawater density, f_0 is the local value of the Coriolis parameter, and β is its meridional gradient. The forcing term is the usual Ekman pumping at the base of the mixed layer; it is related to the wind stress as $W_E = \mathrm{curl}\tau/(\rho_0 f_0)$. The dissipative processes include bottom friction (with coefficient λ) and a Newtonian dissipation (with coefficient κ) of potential vorticity. The streamfunctions are constant [$\psi_i = \psi_{I,b}(t)$, $i = 1, 2$] on the boundaries $\partial\mathcal{D}$ of the domain $\mathcal{D}$ and verify the mass conservation constraint $\iint_{\mathcal{D}} dx\, dy\, (\psi_1 - \psi_2) = \text{const}$ (Larichev 1974; McWilliams 1977; Flierl 1977).

By using the Sverdrup balance and the barotropic Rossby wave period, let us introduce the nondimensional variables:

$$(x, y) \to L_x(x, y), \quad t \to (\beta L_x)^{-1} t, \quad \text{and} \quad \psi \to \tau_0(\rho_0 H\beta)^{-1}\psi = f_0 L_x W_0 (H\beta)^{-1}\psi, \tag{3}$$

where L_x is the zonal width of the basin, $r = L_y/L_x$ is the horizontal aspect ratio, $H = H_1 + H_2$ is the total basin depth, and W_0 is the characteristic amplitude of the Ekman pumping. The two-layer β-value QG equations can then be written as

$$\partial_t[\nabla^2\psi_1 - \mathrm{Bu}^{-1}\delta_2(\psi_1 - \psi_2)] + \beta\partial_x\psi_1 + \alpha J(\psi_1, \psi_{\mathrm{bt}}) + \mathrm{Bu}\alpha J(\psi_1, \nabla^2\psi_1) = \delta_1^{-1} W_E + \nu\nabla^2[\nabla^2\psi_1 - \mathrm{Bu}^{-1}\delta_2(\psi_1 - \psi_2)] \quad \text{and} \tag{4a}$$

$$\partial_t[\nabla^2\psi_2 - \mathrm{Bu}^{-1}\delta_1(\psi_2 - \psi_1)] + \beta\partial_x\psi_2 + \alpha J(\psi_2, \psi_{\mathrm{bt}}) + \mathrm{Bu}\alpha J(\psi_2, \nabla^2\psi_2) = \nu\nabla^2[\nabla^2\psi_2 - \mathrm{Bu}^{-1}\delta_1(\psi_2 - \psi_1)] - \mu\nabla^2\psi_2, \tag{4b}$$

where the Burger number Bu, the baroclinic Rossby radius of deformation R_d, and the scaled layer thicknesses δ_i are defined, respectively, as

$$\mathrm{Bu} = \left(\frac{R_d}{L_x}\right)^2, \quad R_d^2 = \frac{g' H_1 H_2}{f_0^2 H}, \quad \text{and} \quad \delta_i = \frac{H_i}{H}, \tag{5}$$

and the adimensionalized dissipation parameters are given by

$$\nu = \frac{\kappa}{\beta L_x^3} \quad \text{and} \quad \mu = \frac{\lambda}{\beta L_x}. \tag{6}$$

Let us also introduce the barotropic streamfunction defined by

$$\psi_{\rm bt} = \delta_1\psi_1 + \delta_2\psi_2, \tag{7}$$

and the nondimensional forcing parameter

$$\alpha = \frac{f_0 W_0}{\beta^2 R_d^2 H}, \tag{8}$$

which measures the relative contribution to the potential vorticity of the thickness variation of layer 2 due to the wind forcing and the planetary vorticity gradient (Pedlosky 1996, p. 139). The nondimensional parameter $\beta = 1$ is kept to track the origin of the term involved in the algebra of the following sections.

By using typical values for the North Atlantic Ocean midlatitudes: $L_x = 4000$ km, $H = 4000$ m, $R_d = 40$ km, $f_0 = 10^{-4}\ {\rm s}^{-1}$, $\beta = 2 \times 10^{-11}\ {\rm m}^{-1}\ {\rm s}^{-1}$, $W_0 = 2 \times 10^{-6}$ m s^{-1}, and $\kappa = 1000\ {\rm m}^2\ {\rm s}^{-1}$, the nondimensional parameters read ${\rm Bu} = 10^{-4}$, $\alpha = 0.078$, and $\nu = 7.8 \times 10^{-7}$. Comparison with SC03 results should be straightforward, except for some slight differences in the notations and configuration: Our Bu is their ϵ, our α is their γ, and our ν/Bu as shown later for the baroclinic mode dissipation is their ν; their domain extends from $y = [0; 2]$ with two gyres instead of a single gyre extending, here, from $y = [0; r]$.

b. Basinwide scaling

For a basinwide circulation where a small Burger number approximation is valid,

$${\rm Bu} = \left(\frac{R_d}{L_x}\right)^2 \ll 1, \tag{9}$$

Young and Rhines (1982) provided an acclaimed theory for the steady forced–dissipated flow. We propose to jointly study this steady component of the circulation with its time-dependent part. This makes us anticipate as a major feature of our system the interaction between the long baroclinic Rossby waves and the mean barotropic circulation determined by the Sverdrup balance. The flow can be decomposed into a forced–dissipated stationary component $\bar{\psi}$ and a time-dependent component $\tilde{\psi}$, with each of them being also separable into barotropic counterparts as follows:

$$\psi_{\rm bt} = \delta_1\psi_1 + \delta_2\psi_2, \quad \psi_{\rm bc} = \psi_2 - \psi_1, \tag{10}$$

$$\psi_1 = \psi_{\rm bt} - \delta_2\psi_{\rm bc}, \quad \text{and} \quad \psi_2 = \psi_{\rm bt} + \delta_1\psi_{\rm bc}. \tag{11}$$

Using the definitions (10) allows us to end up with the following system:

$$\begin{aligned}\partial_t\nabla^2\psi_{\rm bt} &+ \beta\partial_x\psi_{\rm bt} + {\rm Bu}\alpha J(\psi_{\rm bt}, \nabla^2\psi_{\rm bt}) \\ &+ {\rm Bu}\alpha\delta_1\delta_2 J(\psi_{\rm bc}, \nabla^2\psi_{\rm bc}) \\ &= W_E + \nu\nabla^4\psi_{\rm bt} - \mu\delta_2\nabla^2(\psi_{\rm bt} + \delta_1\psi_{\rm bc}) \quad \text{and}\end{aligned} \tag{12a}$$

$$\begin{aligned}\partial_t({\rm Bu}\nabla^2\psi_{\rm bc} - \psi_{\rm bc}) &+ {\rm Bu}\beta\partial_x\psi_{\rm bc} + {\rm Bu}J(\psi_{\rm bc}, \alpha\psi_{\rm bt}) \\ &+ {\rm Bu}^2(\delta_1^2 - \delta_2^2)J(\psi_{\rm bc}, \nabla^2\psi_{\rm bc}) + {\rm Bu}^2 J(\psi_{\rm bc,}\nabla^2\psi_{\rm bt}) \\ &+ {\rm Bu}^2 J(\psi_{\rm bt}, \nabla^2\psi_{\rm bc}) = -{\rm Bu}\delta_1^{-1}W_E \\ &- {\rm Bu}\mu\nabla^2(\psi_{\rm bt} + \delta_1\psi_{\rm bc}) + \nu\nabla^2({\rm Bu}\nabla^2\psi_{\rm bc} - \psi_{bc}).\end{aligned} \tag{12b}$$

Both baroclinic and barotropic modes satisfy the following boundary conditions:

$$\forall \mathbf{x} \in \delta\mathcal{D}, \quad i \in ({\rm bt}, {\rm bc}), \quad \text{and} \quad \psi_i(\mathbf{x}) = \psi_i^b(t), \tag{13}$$

where ψ_i^b is a real function and depends only on the time variables t; the mass conservation constraint reads

$$\int\int_{\mathcal{D}} dx\, dy\, (\psi_1 - \psi_2) = \int\int_{\mathcal{D}} dx\, dy\, \psi_{\rm bc} = \text{constant}. \tag{14}$$

With no loss of generality, the barotropic streamfunction boundary condition is set at $\psi_{\rm bt} = 0$ on the domain frontier $\delta\mathcal{D}$.

As previously done in Ben Jelloul and Huck (2003) where the method was thoroughly described for the reduced-gravity one-layer QG model, let us solve this system by a weak nonlinear expansion for the streamfunctions of the form

$$\begin{aligned}\psi_{\rm bt} &= \psi_{{\rm bt},0} + {\rm Bu}\psi_{{\rm bt},1} + {\rm Bu}^2\psi_{{\rm bt},2} + \cdots \quad \text{and} \\ \psi_{\rm bc} &= \psi_{{\rm bc},0} + {\rm Bu}\psi_{{\rm bc},1} + {\rm Bu}^2\psi_{{\rm bc},2} + \cdots,\end{aligned} \tag{15}$$

on assuming a multiple time-scale expansion:

$$\partial_t = \partial_{t_0} + {\rm Bu}\partial_{t_1} + {\rm Bu}^2\partial_{t_2} + \cdots. \tag{16}$$

One should note that the time scale for t_1 corresponds to the basin crossing time for baroclinic Rossby waves as used in SC03:

$$T_1 = \frac{T_0}{\rm Bu} = \frac{L_x}{\beta R_d^2}. \tag{17}$$

Let us also define the following notations for specific time average:

$$\overline{f}^{t_i} = \lim_{T_i\to\infty}\frac{1}{T_i}\int_0^{T_i} dt_i\, f(t_0, t_1, \ldots, t_i, \ldots). \tag{18}$$

Last, the steady component of any function f is denoted $\overline{f}$, which is formally equivalent to $\overline{f}^{t_\infty}$.

3. Barotropic Rossby basin modes and steady Sverdrup flow

a. Time-scale separation of basin modes

At first order, (12b) is trivial and enforces the period of the baroclinic Rossby modes to be slower that the barotropic modes:

$$\partial_{t_0}\psi_{\mathrm{bc},0} = 0 \quad \text{and} \quad \psi_{\mathrm{bc},0} = \overline{\psi_{\mathrm{bc},0}}^{t_0}. \tag{19}$$

After canceling the stationary terms at first order in (12a), the inviscid barotropic Rossby wave equation reads for the departure from the stationarity streamfunction $\tilde{\psi}_{\mathrm{bt},0}$:

$$\mathcal{L}^{\mathrm{bt}}\tilde{\psi}_{\mathrm{bt},0} = \partial_{t_0}\nabla^2\tilde{\psi}_{\mathrm{bt},0} + \beta\partial_x\tilde{\psi}_{\mathrm{bt},0} = 0; \tag{20}$$

it is easily solved over the domain and conserves energy since the circulation associated with the basin modes is zero (Pedlosky 1987):

$$\partial_{t_0}\int\int_{\mathcal{D}} dx\, dy\, |\boldsymbol{\nabla}\tilde{\psi}_{\mathrm{bt},0}|^2 = 0. \tag{21}$$

The solution is decomposed into a sum of barotropic Rossby normal modes:

$$\tilde{\psi}_{\mathrm{bt},0} = \sum [A_\Omega(t_1, \ldots)\Phi_\Omega e^{i\Omega t_0} + \text{c.c.}], \tag{22}$$

where c.c. is the complex conjugate of each term to keep the solution real; they satisfy

$$\mathcal{L}^{\mathrm{bt}}_\Omega\Phi_\Omega = \mathrm{i}\Omega\nabla^2\Phi_\Omega + \beta\partial_x\Phi_\Omega = 0 \quad \text{and}$$
$$\frac{1}{2r}\int\int_{\mathcal{D}} dx\, dy\, |\boldsymbol{\nabla}\Phi_\Omega|^2 = 1. \tag{23}$$

The analytical solution from the classical paper by Longuet-Higgins (1964) and textbook by Pedlosky (1987) is

$$\Phi_\Omega = D_\Omega \exp\left(\frac{i\beta x}{2\Omega}\right) \sin m\pi x \sin\frac{n\pi y}{r}, \tag{24a}$$

where

$$D_\Omega = \frac{4\Omega}{\beta} \quad \text{and} \quad \Omega = \frac{\beta}{2\pi\sqrt{m^2 + n^2 r^{-2}}}. \tag{24b}$$

b. Stationary solution

1) Sverdrup flow

Averaging the first-order evolution equation yields the steady-state solution:

$$\beta\partial_x\overline{\psi}_{\mathrm{bt},0} = W_E + D, \tag{25}$$

where the overbar denotes averaging over all time scales t_i. The solution is composed of an inviscid Sverdrup interior circulation and a thin western boundary current where the dissipation D is active. Some friction, whatever its type, is needed to dissipate the potential vorticity input: this occurs in a western boundary layer whose thickness is controlled by the dissipation coefficient. In the following and except when specifically mentioned, we will assume that dissipation is strong enough to stabilize the strong western boundary current. Moreover, the basin zonal width will be also assumed to be sufficiently large relative to the western boundary layer thickness. These hypotheses allow us to write

$$\overline{v}_{\mathrm{bt},0} = \partial_x\overline{\psi}_{\mathrm{bt},0} = \beta^{-1}W_E - \beta^{-1}\delta(x)\int_0^1 dx\, W_E, \tag{26}$$

where δ is the Dirac distribution and represents the strongly localized western boundary current. The streamfunction is thus expressed as

$$\overline{\psi}_{\mathrm{bt},0} = \beta^{-1}W_E[x - H(x)], \tag{27}$$

where $H(x)$ is the Heaviside function. In the expression of the meridional velocity (26), the western boundary current is crudely represented by a delta function. A finite width would be allowed by changing the delta function into $f(x/\Delta)/\Delta$ where the function f, satisfying $\int_0^\infty du\, f(u) = 1$, reflects the boundary current structure and Δ its width. For example, Stommel's solution corresponds to a function $f(x/\Delta) = \exp(-|x|/\Delta)$, where $\Delta = \mu/\beta$. In the following we will consider the academic rectangular basin geometry where the Ekman pumping satisfies

$$\forall \mathbf{x} \in \mathcal{D} = [0, 1] \times [0, r] \quad \text{and}$$
$$W_E(x, y) = W_E(y) = -\sin\frac{k\pi y}{r}. \tag{28}$$

This Ekman pumping is typical of the North Atlantic subtropical single gyre ($k = 1$) and subtropical–subpolar double-gyre system ($k = 2$).

At next order in Bu, the system (12) reduces to

$$\mathcal{L}^{\mathrm{bt}}\psi_{\mathrm{bt},1} + \partial_{t_1}\nabla^2\psi_{\mathrm{bt},0} + J(\psi_{\mathrm{bt},0}, \nabla^2\psi_{\mathrm{bt},0}) + 2\delta_2\delta_1 J(\psi_{\mathrm{bc},0,}\nabla^2\psi_{\mathrm{bc},0}) = 0 \quad \text{and} \tag{29a}$$

$$\partial_{t_0}Q\psi_{\mathrm{bc},1} + \partial_{t_1}Q\psi_{\mathrm{bc},0} + J(\psi_{\mathrm{bc},0,}\alpha\psi_{\mathrm{bt},0} + \beta y) + \delta_1^{-1}W_E = 0, \tag{29b}$$

where the dissipative terms are neglected, and the linear operators $\mathcal{L}^{\mathrm{bt}}$ and Q are defined by

$$Qf = \mathrm{Bu}\nabla^2 f - f \quad \text{and} \quad \mathcal{L}^{\mathrm{bt}}f = \partial_{t_0}\nabla^2 f + \beta\partial_x f. \tag{30}$$

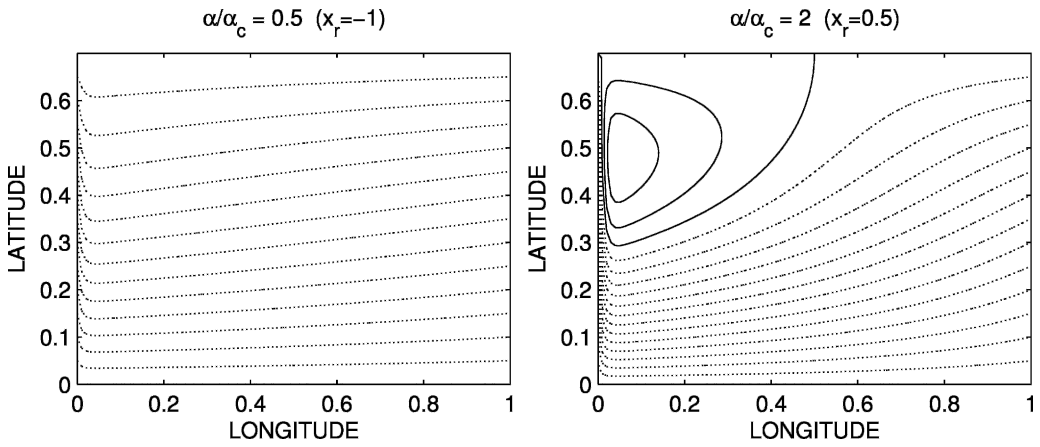

FIG. 1. Geostrophic contours for two different values of the forcing strength (α/α_c = 1/2 and 2). Contour interval is 0.05 in nondimensional units, and positive (negative) contours are solid (dotted). Since the β-plane quasigeostrophic potential vorticity contours are defined up to an additive constant, we choose the latter so that the zero line corresponds to the northern boundary.

It is worth noting that we kept the higher-order term appearing here as a linear dispersive term. This will be commented upon later.

Averaging (29b) over time t_0 yields

$$\partial_{t_1} Q\psi_{\mathrm{bc},0} + J(\psi_{\mathrm{bc},0}, \alpha\overline{\psi_{\mathrm{bt},0}}^{t_0} + \beta y) + \delta_1^{-1} W_E = 0. \quad (31)$$

Further averaging of (31) provides an additional equation to (25) and closes the steady forced–dissipated problem:

$$J(\overline{\psi}_{\mathrm{bc},0}, \alpha\overline{\psi}_{\mathrm{bt},0} + \beta y) + \delta_1^{-1} W_E = 0. \quad (32)$$

2) YOUNG AND RHINES (1982) THEORY

This system was solved by Young and Rhines (1982) and their solution consists of a barotropic flow satisfying the Sverdrup balance except in a thin western boundary layer. In the case of closed geostrophic contours, that is, contours of $\alpha\overline{\psi}_{\mathrm{bt},0} + \beta y$, the baroclinic structure of the gyre is such that the lower layer is at rest, except in a recirculating pool where potential vorticity is homogenized. This pool can exist only when the zonal barotropic transport is sufficiently strong (Pedlosky 1996; Fig. 1); that is,

$$\alpha > \alpha_c = \frac{\beta r}{k\pi}. \quad (33)$$

Fulfillment of this condition gives the maximal zonal extent of the pool as $x_r = 1 - \beta r/(k\alpha\pi)$. The solution can then be summarized as follows: outside the pool it is

$$\overline{\psi}_{\mathrm{bt}} = \beta^{-1} \int_{x_e}^{x} dx\, W_E, \quad \overline{\psi}_{\mathrm{bc,YR}} = -\delta_1^{-1}\overline{\psi}_{\mathrm{bt}}, \quad \text{and} \quad (34)$$

$$\overline{\psi}_{1,\mathrm{YR}} = \delta_1^{-1}\overline{\psi}_{\mathrm{bt}},\ \overline{\psi}_{2,\mathrm{YR}} = 0, \quad (35)$$

whereas inside the pool it becomes

$$\overline{\psi}_{\mathrm{bt}} = \beta^{-1} \int_{x_e}^{x} dx\, W_E, \quad \overline{\psi}_{\mathrm{bc,YR}} = \delta_1^{-1}\beta(y - y_n), \quad (36)$$

$$\overline{\psi}_{1,\mathrm{YR}} = \delta_1^{-1}(1 - \delta_2\alpha)\overline{\psi}_{\mathrm{bt}} - \delta_2\delta_1^{-1}\beta(y - y_n), \quad \text{and}$$

$$\overline{\psi}_{2,\mathrm{YR}} = \alpha\overline{\psi}_{\mathrm{bt}} + \beta(y - y_n), \quad (37)$$

where $x_e = 1$ is the longitude of the basin eastern boundary and $y_n = r$ is the latitude of its northern boundary.

One should note that this solution needs some friction between the two layers to mix the lower layer potential vorticity, but setting this dissipation to an arbitrary low value has no effect on the resulting solution (36). These considerations led us to neglect friction at least at the first order of the time-varying part.

3) GENERAL INVISCID SOLUTION

Rewriting (32) by using (25) yields

$$J(\overline{\psi_{\mathrm{bc},0}}^{t_1} + \delta_1^{-1}\overline{\psi}_{\mathrm{bt},0}, \alpha\overline{\psi}_{\mathrm{bt},0} + \beta y) = 0, \quad (38)$$

where the partial time average is the one defined above. The general solution becomes

$$\overline{\psi_{\mathrm{bc},0}}^{t_1} = f(\overline{\psi}_{\mathrm{bt},0} + \beta y) - \delta_1^{-1}\overline{\psi}_{\mathrm{bt},0}, \quad (39)$$

where f is an arbitrary, still undetermined, real-valued function. The use of partial fast-time average instead of an absolute time average is essentially a matter of mathematical rigor; both are equivalent here as we do not analyze any higher-order interaction acting on time scales longer than t_1. The Young and Rhines (1982)

solution is actually a particular case of the general equation in (39) for the function $f(x) = \delta_1^{-1}x$.

4. Baroclinic basin modes

Before focusing on the baroclinic component of the flow, let us briefly describe the results issued from the barotropic equation in (29a). Elimination of resonances provides an amplitude equation for any barotropic basin mode and highlights the interaction between the barotropic basin modes and the Sverdrup flow. The complete analysis was given in Ben Jelloul and Huck (2003). To compute the nonresonant fields, it is convenient to use the following notations:

$$\psi_{\mathrm{bt},1} = \sum [A_1(\Omega; t_1, \ldots)\Phi_\Omega e^{i\Omega t_0} + A_1(2\Omega; t_1, \ldots)\Phi_{2\Omega} e^{i2\Omega t_0} + \mathrm{c.c.}] + \overline{\psi_{\mathrm{bt},1}}^{t_0}, \tag{40}$$

where $\overline{\psi_{\mathrm{bt},1}}^{t_0}$ is the slow component, which evolves on time scale t_1, of the first correction to the barotropic flow. The biharmonic contribution satisfies

$$A_1(2\Omega; t_1, \ldots) = A_0^2(\Omega) \quad \text{and}$$
$$\Phi_{2\Omega} = -(\mathcal{L}^{\mathrm{bt}}_{2\Omega})^{-1} J(\Phi_\Omega, \nabla^2\Phi_\Omega), \tag{41}$$

where the linear anti-Hermitian operator $\mathcal{L}_{2\Omega}$ is defined by

$$\mathcal{L}^{\mathrm{bt}}_{2\Omega} = 2i\Omega\mathcal{Q} + \beta\partial_x. \tag{42}$$

The remaining nonresonant terms force the slow evolution of the order-one perturbation:

$$\overline{\psi_{\mathrm{bt},1}}^{t_0} = -[\overline{J(\psi_{\mathrm{bt},0}, \nabla^2\psi_{\mathrm{bt},0})}^{t_0} + 2\delta_1\delta_2 J(\psi_{\mathrm{bc},0}, \nabla^2\psi_{\mathrm{bc},0})]. \tag{43}$$

This last expression depends on the baroclinic component whose detailed analysis is provided below.

An orthogonal base of advected baroclinic Rossby basin modes

The baroclinic modes equation is obtained from (31) by canceling the stationary contributions:

$$\partial_{t_1}(\mathrm{Bu}\nabla^2\tilde{\psi}_{\mathrm{bc},0} - \tilde{\psi}_{\mathrm{bc},0}) + J(\tilde{\psi}_{\mathrm{bc},0}, \tilde{\psi}_{\mathrm{bt},0} + \beta y) = 0. \tag{44}$$

Integration over the whole domain by using the mass conservation (14) and the boundary conditions (13) yields

$$\partial_{t_1} \oint_{\delta\mathcal{D}} \tilde{\mathbf{u}}_{\mathrm{bc}} \cdot d\mathbf{s} = -\tilde{\psi}^b_{\mathrm{bc},0} \oint_{\delta\mathcal{D}} \frac{\partial(\overline{\psi}_{\mathrm{bt},0} + \beta y)}{\partial \mathbf{s}} \cdot d\mathbf{s} = 0, \tag{45}$$

where $\tilde{\mathbf{u}}_{\mathrm{bc}} = (-\partial_y\tilde{\psi}_{\mathrm{bc},0}, \partial_x\tilde{\psi}_{\mathrm{bc},0})$; this is the conservation of the circulation associated with the oscillating baroclinic function. The system (44) being linear and autonomous, we look for solutions separable in space and time, in the modal form: $\tilde{\psi}_{\mathrm{bc},0} = \exp(\sigma t)\phi(x, y)$. If $\tilde{\mathrm{u}}_{\mathrm{bc}}$ is the velocity of such an eigenmode associated with a nonvanishing eigenvalue σ, its circulation must be zero by (45).

One can easily check that the mode energy is conserved since the barotropic steady flow has only an advective action on the baroclinic streamfunction at this order of the expansion [multiply (44) by $\tilde{\psi}_{\mathrm{bc},0}$ and integrate over the domain with the appropriate boundary conditions].

Equation (44) can be rewritten as follows:

$$\mathcal{Q}^{-1}\mathcal{L}^{\mathrm{bc}}\tilde{\psi}_{\mathrm{bc},0} = \partial_{t_1}\tilde{\psi}_{\mathrm{bc},0} + \mathcal{Q}^{-1}\mathcal{T}\tilde{\psi}_{\mathrm{bc},0} = 0, \tag{46}$$

where the linear operators $\mathcal{T}$ and $\mathcal{L}^{\mathrm{bc}}$ are defined by

$$\mathcal{T}f = J(f, \overline{\psi}_{\mathrm{bt},0} + \beta y) \quad \text{and} \quad \mathcal{L}^{\mathrm{bc}} = \partial_{t_1}\mathcal{Q} + \mathcal{T}. \tag{47}$$

Defining

$$\langle f|g\rangle_{\mathcal{Q}} = -\frac{1}{2r}\int\int_{\mathcal{D}} dx\, dy\, fQg = \frac{1}{2r}\int\int_{\mathcal{D}} dx\, dy\, (\mathrm{Bu}\boldsymbol{\nabla}f\cdot\boldsymbol{\nabla}g + fg) + \frac{1}{2r}\oint_{\delta\mathcal{D}} ds\, \mathrm{Bu}f(\mathbf{n}\cdot\boldsymbol{\nabla}g) \tag{48}$$

provides a scalar product for the space of streamfunctions that are constant on the boundaries and have zero circulation since the last contour integral can be rewritten as

$$\oint_{\delta\mathcal{D}} ds\, f(\mathbf{n}\cdot\boldsymbol{\nabla}g) = f\oint_{\delta\mathcal{D}} ds\, (\mathbf{n}\cdot\boldsymbol{\nabla}g) = f\oint_{\delta\mathcal{D}} \mathbf{u}_g\cdot d\mathbf{s} = 0, \tag{49}$$

where $\mathbf{u}_g = (-\partial_y g, \partial_x g)$ is the velocity associated with the streamfunction g.

The operator $\mathcal{Q}^{-1}\mathcal{T}$ is antisymmetric for the previously defined scalar product metric; it is thus diagonal in a base of orthogonal eigenvectors ϕ_ω with purely imaginary eigenvalues $i\omega$ satisfying

$$i\omega\phi_\omega = -\mathcal{Q}^{-1}\mathcal{T}\phi_\omega. \tag{50}$$

This property allows us to conclude about the purely oscillating nature of the baroclinic modes on time scale t_1 and write solution for the baroclinic mode as

$$\tilde{\psi}_{\mathrm{bc},0} = \sum_{\omega\in S_{\mathrm{bc}}} [B_0(\omega; t_2, \ldots)\phi_\omega e^{i\omega t_1} + \mathrm{c.c.}], \tag{51}$$

where $S_{\rm bc}$ is the spectrum of the eigenvalues. The normal modes ϕ_ω satisfy

$$\mathcal{L}_\omega^{\rm bc}\phi_\omega = i\omega Q\phi_\omega + \mathcal{T}\phi_\omega = 0 \quad \text{and}$$
$$-\int\int_D dx\,dy\;\phi_\omega Q\phi_\omega = 1, \tag{52}$$

which result from the normalization of the modes by their energy value.

In contrast with the study by Spydell and Cessi (2003) where only dissipation was retained to enforce the correct boundary conditions, we kept the higher-order dispersion term in (44) because it is the only one that enables the solution to satisfy the western boundary condition in the presence of advection by mean flow. With no dispersion, the phase crests starting from the meridional eastern boundary reaches the western boundary with a nonrectilinear shape resulting from differential advection by the Sverdrup flow. Thanks to dispersion, short Rossby waves have an eastward group velocity; hence the reflection of westward long Rossby waves at the western boundary generates short Rossby waves, and their superposition satisfies the no-flow boundary condition.

Equation (44) can also be seen as the propagation of baroclinic Rossby waves in an inhomogeneous planetary vorticity gradient. By studying the long-wave limit for Rossby modes in inhomogeneous potential vorticity gradient in a basin with a large meridional extent, where the β-plane assumption is no longer valid (no background mean flow), Cessi and Louazel (2001) found not only that these modes are more damped, but also that higher modes are more damped than lower ones. The latter results from the dephasing experienced at the western boundary by an initial rectilinear north–south crest emanating from the eastern boundary. The greater dephasing experienced by higher modes leads to a decay rate proportional to the mode wavenumber m. One may wonder how a simple linear mode can be damped with neither mean flow to feed or be fed by higher-frequency modes, nor dissipation since the Coriolis force does not work. Cessi and Louazel (2001) and SC03 both connected the inviscid interior solution to boundaries by solving the dissipative boundary layer at the western boundary. This mechanism was also examined in nonrectangular basins by Primeau (2002) and LaCasce and Pedlosky (2002). One may prefer the effect of dispersion to satisfy the boundary conditions and reject dissipation processes at higher orders (especially for theoretical purposes); this procedure would allow one to study destabilizing nonlinear interactions as well as stabilizing dissipation effects at the same higher order—this issue will be addressed elsewhere.

Last, one should note that the limit $\mathrm{Bu} = R_d = 0$ is singular since it implies that the gravity or the full depth is zero.[1] Physically the Rossby radius is a cutoff scale below which the fields somehow are smoothed; taking it equal to zero yields singular solutions. Therefore, the Burger number and Rossby radius can be assumed as small as needed, but must remain finite.

5. Numerical resolution and baroclinic typology

Frequencies and spatial structure of the modes are numerically computed from (50). We solve the generalized eigenvalue problem arising from finite differentiating (44), as done by Cessi and Primeau (2001):

$$\begin{aligned} i\omega(\mathrm{Bu}\nabla^2\phi_\omega - \phi_\omega) = &-(\beta + \alpha\partial_y\overline{\psi}_{\mathrm{bt},0})\partial_x\phi_\omega \\ &+ \alpha\partial_x\overline{\psi}_{\mathrm{bt},0}\partial_y\phi_\omega \\ &+ \nu\mathrm{Bu}^{-1}\nabla^2(\mathrm{Bu}\nabla^2\phi_\omega - \phi_\omega), \end{aligned} \tag{53}$$

using Arnoldi's method as provided in "ARPACK" (Lehouck et al. 1998) for a prescribed number of eigenvalues (typically 100) with the largest real part. Downgradient potential vorticity eddy diffusion is needed to avoid grid point structures and isolate large-scale modes through their lower damping rate. Our numerical procedure differs from the spectral method used by Spydell and Cessi (2003) because they projected (53) on a base of Jacobi polynomials well suited for resolving dissipative layers at the domain boundary. On the other hand, our spatial resolution is uniform and allows accurate resolution of structures with internal boundary layers like the ones appearing on the edge of the closed geostrophic contours pool.

Our equations conserve dispersion as an alternative regularizing mechanism, even if their resolution requires a small dissipation for numerical convergence and mode selection in the case of a realistically small Burger number.

A fundamental result is that, depending on the forcing strength, the spectrum of the linear operator admits a qualitative transition. All following calculations were made with oceanically relevant parameters: $\mathrm{Bu} = 10^{-4}$, $r = 0.7$, and $\upsilon/\mathrm{Bu} = 10^{-3}$ on a 100×100 grid; α, representing the forcing strength, hence the barotropic streamfunction amplitude, was the varying parameter. Moreover, the barotropic flow was assumed to be a single gyre flow with a Munk-type boundary layer of nondimensional thickness equal to 0.05 (5 grid points).

We made additional calculations in order to clarify

[1] Note that the limit $\mathrm{Bu} = R_d = \infty$ can be fulfilled and yields to Euler equation on the β plane.

TABLE 1. Influence of dissipation on the largest-scale modes damping rate and frequency (eigenvalue $i\omega$ is provided) as a function of Burger number for $\alpha/\alpha_c = 1/2$ (R is deformed Rossby basin mode followed by zonal and meridional wavenumbers). In the inviscid case, the real part of the eigenvalue largely varies with the resolution: it decreases to -2.8×10^{-5} for 200×200 grid points and -1.2×10^{-5} for 300×300 grid points.

Bu:	10^{-4}		10^{-2}
ν	R 2 × 1	R 3 × 1	R 2 × 1
0	—	—	$-1.1 \times 10^{-4} \pm 4.706i$
10^{-4}	$-0.623 \pm 6.079i$	$-1.088 \pm 13.551i$	$-0.042 \pm 4.695i$
10^{-3}	$-0.760 \pm 5.958i$	$-1.643 \pm 13.487i$	$-0.275 \pm 4.639i$
10^{-2}	$-1.486 \pm 5.751i$	$-3.840 \pm 12.191i$	$-2.237 \pm 4.001i$
10^{-1}	$-7.011 \pm 5.365i$	$-19.306 \pm 9.578i$	—

the relative influence of dispersion and dissipation for two typical forcing values (Tables 1 and 2). We also performed one-dimensional calculations to estimate the sensitivity of the results to the horizontal resolution, which could hardly be increased in two dimensions since the $(100 \times 100)^2$ eigenvalue problem already requires several gigabytes of memory. All together, these results show that friction always controls the damping rate, even when it is small relative to dispersion (see column Bu = 10^{-2} in Tables 1 and 2). Therefore and in agreement with our analytical results, we expect all modes to become neutral in the inviscid limit. We verified it numerically for Bu = 10^{-2}; indeed, in this case, we resolved the inviscid eigenmodes thanks to the separation of mode frequencies by dispersion. However, when the Burger number tends to zero, the Rossby deformation radius becomes smaller than the resolved scales; smaller scales thus appear in the western boundary, but their strong dissipation enhances damping. In addition, dispersion becomes too weak to allow the separation of eigenmodes with the same zonal wavenumber but different meridional structures (all of them have almost the same eigenvalue). We speculate that, if we had been able to actually resolve such scales (i.e., low-frequency small-scale Rossby waves) and accordingly reduce the friction coefficient, we would have separated the modes and the damping rate would have tended to zero. This conjecture contrasts with SC03 results where dispersion was neglected. Last, our one-dimensional calculations suggest that only the larger-scale modes are well resolved in our analysis; discrepancies exceeding 10% between poorly and well-resolved modes are thus expected in frequency, damping rate, and especially spatial structure for wavenumbers higher than 5.

a. Deformed Rossby basin modes (shadow modes)

With no forcing the eigenmodes can be classified into two branches (Larichev 1974; LaCasce and Pedlosky 2002): the former consists in modes with streamfunction vanishing on the boundaries with dispersion relation

$$\Omega = \frac{\beta \mathrm{Bu}^{-1}}{2\sqrt{\mathrm{Bu}^{-1} + \pi^2(m^2 + n^2 r^{-2})}}, \tag{54}$$

and a spatial structure similar to the barotropic one (24a), but only the modes with vanishing volume, that is, those with even n, have to be kept. The latter is formed of modes with nonvanishing streamfunction on

TABLE 2. Influence of dissipation on the largest-scale modes damping rate and frequency (eigenvalue $i\omega$ is provided) as a function of Burger number for $\alpha/\alpha_c = 1.5$ (R is deformed Rossby basin mode, P is oscillatory recirculating mode, and S is stationary pool mode, followed by zonal—or along potential vorticity contours—and meridional—or across potential vorticity contours—wavenumbers). In the inviscid case, the real part of the eigenvalue largely varies with the resolution: it decreases to -5.6×10^{-6} for 200×200 grid points, and -2.5×10^{-6} for 300×300 grid points.

Bu:	10^{-4}			10^{-2}
ν	R 2 × 1	P 1 × 1	S 1	R 2 × 1
0	—	—	—	$-2.2 \times 10^{-5} \pm 6.272i$
10^{-4}	$-1.059 \pm 8.224i$	$-0.194 \pm 2.618i$	-0.058	$-0.073 \pm 6.253i$
3×10^{-4}	$-1.322 \pm 8.117i$	$-0.501 \pm 2.569i$	-0.164	$-0.169 \pm 6.218i$
10^{-3}	$-1.548 \pm 7.951i$	$-1.094 \pm 2.492i$	-0.410	$-0.448 \pm 6.135i$
3×10^{-3}	$-2.017 \pm 7.679i$	$-2.581 \pm 2.577i$	-1.093	$-1.101 \pm 5.868i$
10^{-2}	$-2.879 \pm 6.864i$	$-5.122 \pm 3.218i$	-2.554	$-2.653 \pm 5.018i$
10^{-1}	$-7.651 \pm 5.604i$	$-22.97 \pm 2.420i$	-11.132	—

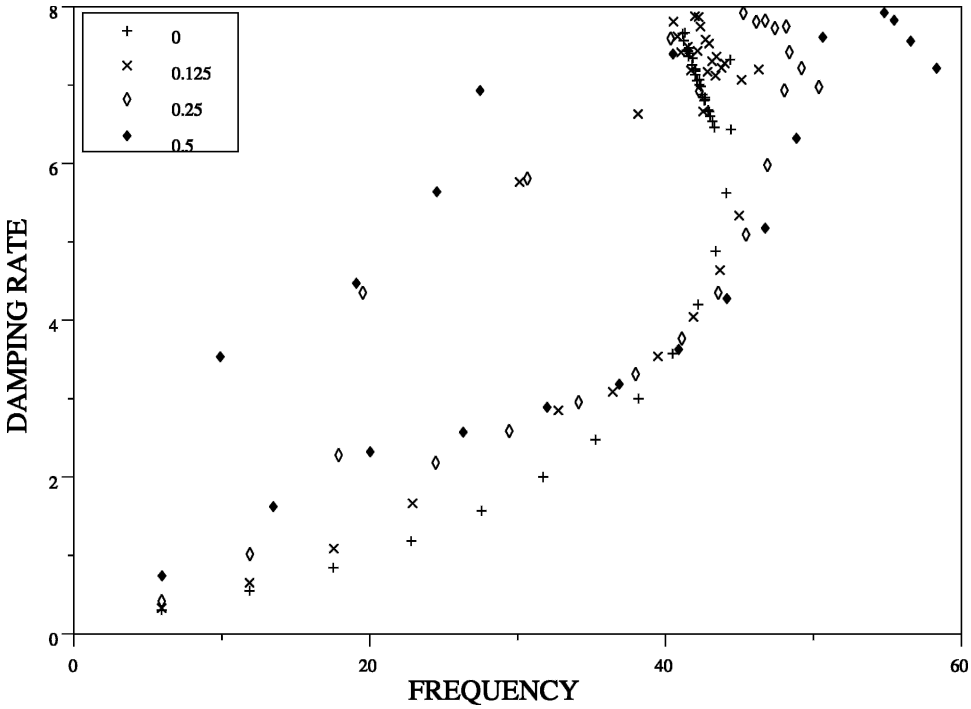

FIG. 2. Frequencies and damping rates for four different weak barotropic flows. Frequencies are in abscissa, and damping rates are in ordinate. The value of α/α_c is indicated for each case.

the boundaries: in the limit of vanishing Burger number, they are large zonal-scale low-frequency modes (LaCasce 2000; Cessi and Primeau 2001).

Under weak forcing, that is, $\alpha < \alpha_c$, the geostrophic contours are not closed, as seen above (Fig. 1). Deformed Rossby basin modes (or shadow modes), which are the continuous extension of the classical Rossby modes (i.e., the neutral linear perturbation of a resting ocean), are obtained for a nonzero Sverdrup flow. Their periods are about the time spent by a large-scale Rossby wave to travel across the basin; that is, $L_x/(\beta R_d^2)$ for the first zonal mode, and its divisors for higher zonal wavenumber modes ($\omega_m = 2\pi m$). Figure 2 illustrates frequencies and damping rates computed in the case of a single subtropical gyre and different weak forcings.

The large-scale low-frequency Rossby basin modes are deformed by the barotropic flow: they are accelerated (slowed) in the southern (northern) half of the basin. Moreover, the modes with higher zonal wavenumbers show a reduction of their corresponding wave speed due to stronger dispersion and are arrested earlier when propagating westward (Fig. 3).

One should note the occurrence of modes other than the large-scale low-frequency ones with really close frequencies. In our opinion, they result from a combination of large-scale low-frequency modes with higher meridional wavenumbers; indeed, the latter have very similar frequencies at small Bu, but are more heavily damped with no barotropic flow. When it is present, the barotropic flow couples them to the meridionally gravest ones. This coupling actually occurs between all modes, but is more efficient when modes are of comparable frequencies. For example, let us focus on the two couples of modes near the frequencies $2 \times 2\pi$ and $3 \times 2\pi$ for $\alpha/\alpha_c = 1/2$ (Fig. 4). Their occurrence likely results from a coupling between original modes differing by their meridional wavenumbers; these modes form a quasi-degenerate spectrum for small Bu in the inviscid case. Moreover, the faster (slower) mode of the couple coincides with a stronger signal in the southern (northern) part of the basin where it is accelerated (slowed) by the barotropic flow.

This process exhibits similarities with the "bouncing" of the shadow modes discussed in SC03, although we cannot here strictly follow an eigenmode and its associated eigenvalue through varying forcing. Like the bouncing, the coupling occurs when two basin modes with consecutive wavenumbers converge to the same eigenvalue at increasing forcing: this transition happens when the lower-order eigenmode meridional wavenumber shifts along the western boundary.

For higher forcing $\alpha > \alpha_c$, the basin modes are deformed by the mean flow such that they are completely expelled from the region where Rossby waves cannot

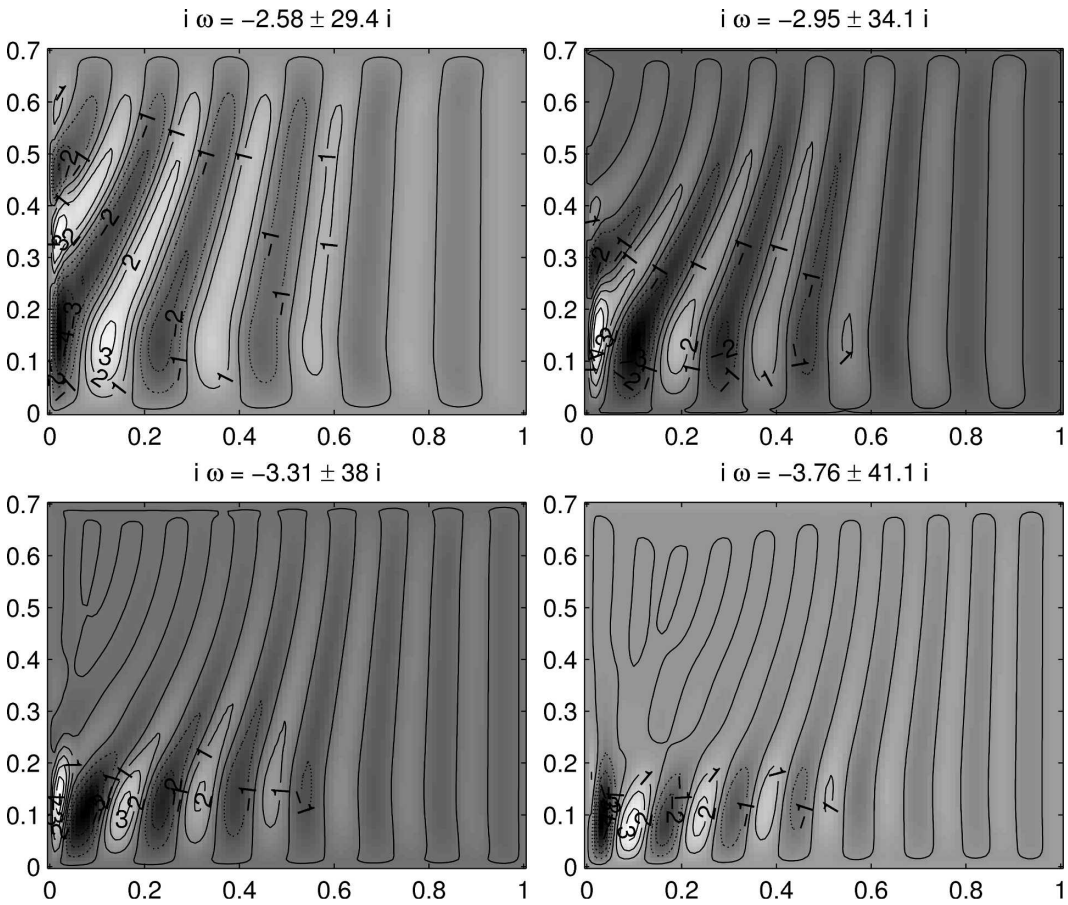

FIG. 3. Low-frequency Rossby basin modes for weak barotropic flow $\alpha/\alpha_c = 0.25$. Only one phase of each oscillatory mode is shown. Axes are longitude and latitude in nondimensional units. Note that the exclusion zone grows with the zonal wavenumber.

propagate westward (Fig. 5). Note that the modes with higher zonal wavenumbers are expelled from a larger part of the domain: It is expected that higher-order modes are more dispersive; thus the corresponding baroclinic Rossby waves velocity is weaker and the modes are arrested earlier, as above, but this effect seems here independent of the Burger number as it tends to zero (as suggested by an anonymous reviewer). These considerations made us propose the following alternative. The dissipation scale is a function of the friction coefficient only: $k_d \propto \nu/\mathrm{Bu}$. The frequency ω of the mode enforces a relation between the wavenumber k and the local background potential vorticity gradient $(\beta - U)$ through the dispersion equation all along the wave propagation, from the eastern boundary (where $k = k_0$ function of ω, and $U = 0$) to the region where it vanishes through dissipation (where $k = k_d$ and $U > 0$). Hence the larger k_0 is, the weaker U the wave can sustain before being dissipated and the farther eastward its propagation is arrested. A simple analogy can be made in one dimension for the nondispersive inviscid dispersion relation: $-i\omega\phi = -a(x - x_r)\partial_x\phi$, where x_r is the abscissa of the separatrix and a measures the intensity of the circulation such that $\beta - U \simeq a(x - x_r)$. The analytical solution is $\exp[i(\omega/a)\ln(x - x_r)]$ and shows very clearly the increase of the wavenumber as the wave propagates westward toward the separatrix. For modes with higher frequency ω, these shorter scales develop farther away from the separatrix; in the complete solution, they would be undoubtedly heavily damped by the dissipation, expelling the associated mode from larger regions around the pool.

Spydell and Cessi (2003) found similar modes (named shadow modes) with main differences in the western part of the basin and enhanced oscillations in the vicinity of the critical line consisting of the pool frontier. Such differences may result from their numerical method that enhances the resolution close to the domain boundaries, but remains maladjusted for the pool frontier (it is difficult to compare the resolution in

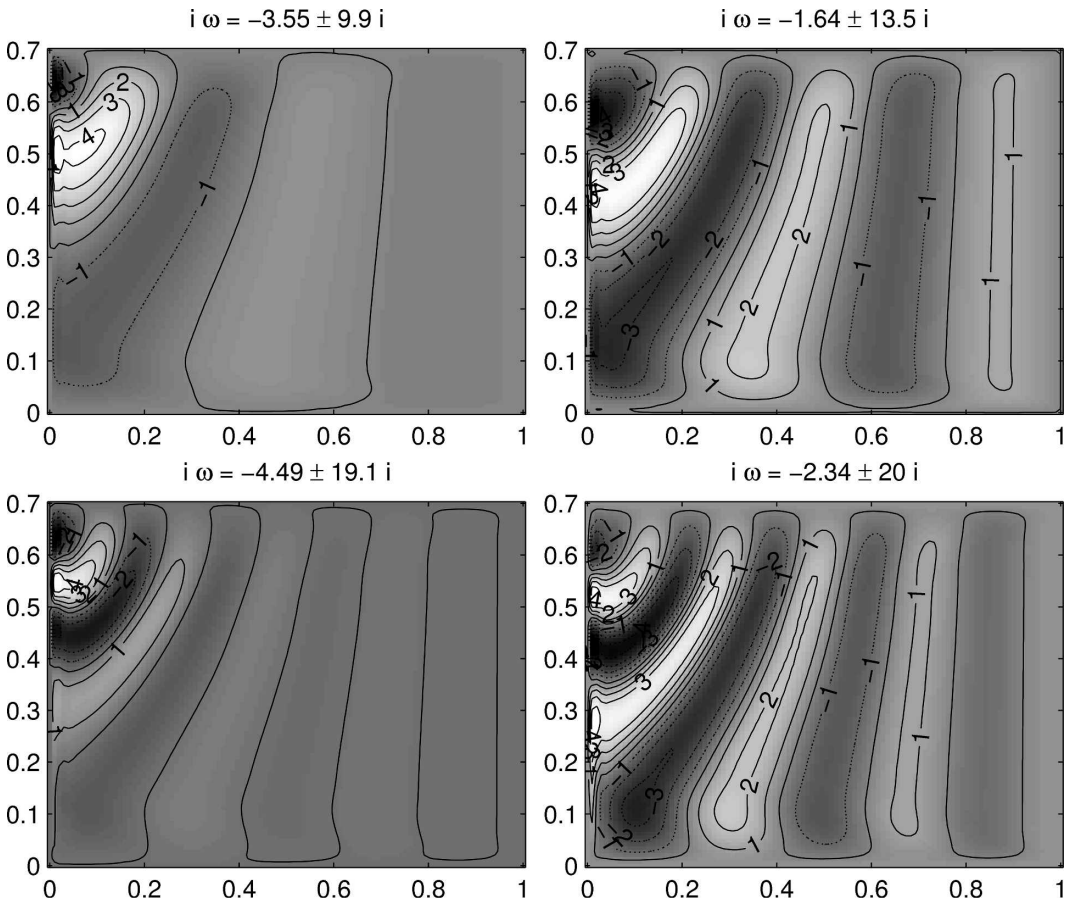

FIG. 4. Coupling of quasi-degenerate modes with frequencies around 4π and 6π for $\alpha/\alpha_c = 1/2$. Only one phase of each mode is shown. Axes are longitude and latitude in nondimensional units. Note the intensification in the northwestern (southwestern) part for the lowest (highest) frequency mode.

the domain interior since the number of Jacobi polynomials used in their study is not provided).

b. Recirculating pool modes

When the condition (33) for the existence of a recirculating pool is fulfilled, that is, for sufficiently strong forcing, new modes with lower frequencies appear in addition to the deformed Rossby basin modes, as shown in Fig. 6. In Fig. 7 the different types of modes are individuated for $\alpha/\alpha_c = 2$.

Oscillating recirculating modes appear when a recirculation gyre is formed. They consist of advection-dominated waves trapped within the pool where they propagate along closed contours of potential vorticity. In analogy with Rossby basin modes, they can be indexed by their wavenumbers by considering, now, the azimuthal and radial wavenumbers inferred from mode envelope $|\phi_\omega|$. For a given azimuthal wavenumber, the mode period is increasing with higher radial wavenumber since dispersion acts as a decelerator. Furthermore, Fig. 8 shows that for azimuthal wavenumber 2, the mode period is about the divisor of the first azimuthal mode.

Several computations in the double gyre case (not shown) highlighted the occurrence of the same recirculating modes in each gyre, up to a change of sign producing symmetric and antisymmetric recirculating modes.

By neglecting the dispersive terms in (44), the baroclinic mode behaves like a passive tracer advected by an inviscid flow with streamfunction $\alpha\overline{\psi}_{\mathrm{bt},0} + \beta y$. We numerically checked that a particle near the center of the gyre is more rapidly advected than at the edge. Thus, evaluating the time spent by a particle to recirculate at the gyre center yields the requested time scale. The aforementioned time can be decomposed into two parts as a quasi-instantaneous travel in the western boundary current (considered infinitely thin and fast) and the time spent in a semicircular trajectory in the gyre. The latter can be evaluated as $\pi/(\zeta/2)$, where ζ is the vorticity

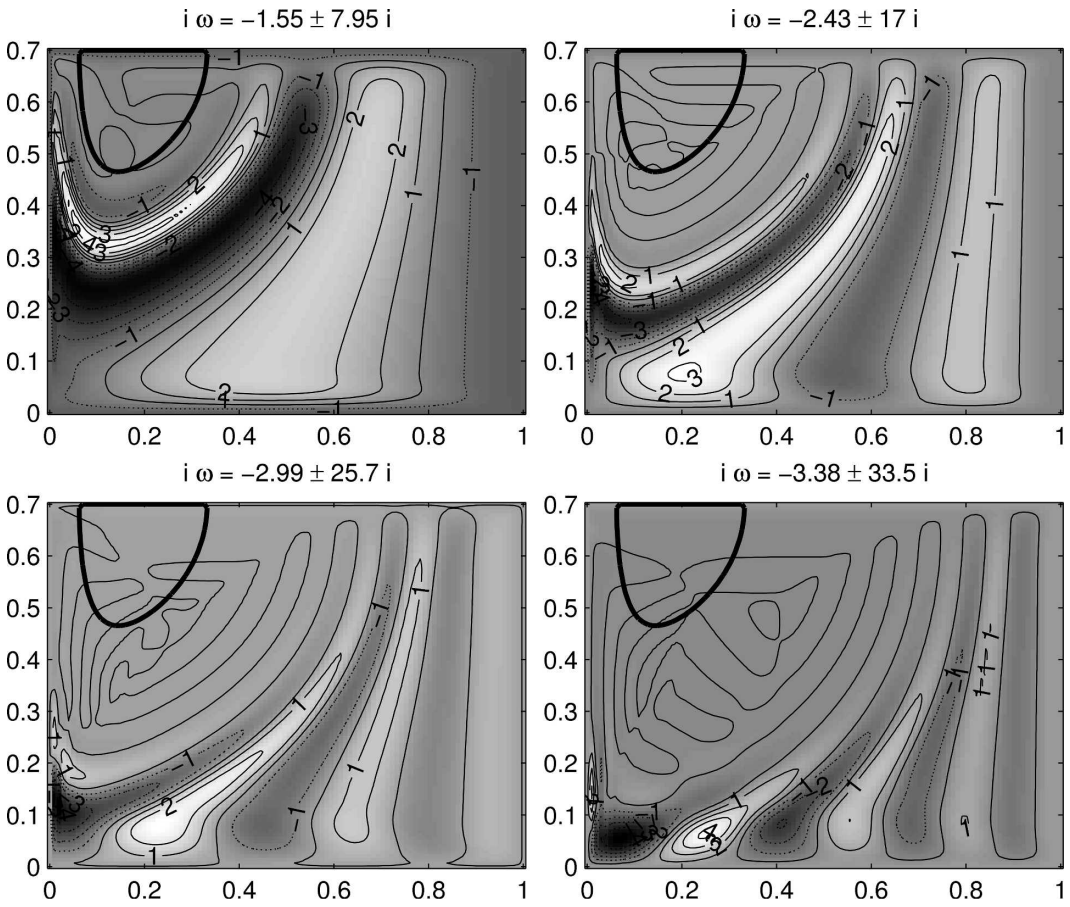

FIG. 5. Low-frequency large-scale Rossby basin modes arrested by the mean flow in the northwestern region of the basin for $\alpha/\alpha_c = 1.5$. Only one phase of each mode is shown. The zero contour line indicates the limit of the closed geostrophic contours pool. Axes are longitude and latitude in nondimensional units.

at the gyre center (and thus $\zeta/2$ is the rotation rate). The gyre center coordinates are easily computed:

$$x_c = 0 \quad \text{and} \quad y_c = \frac{r}{\pi} \arccos \frac{\beta r}{\pi \alpha}, \tag{55}$$

and yield the value of the vorticity:

$$\zeta = \nabla^2(\alpha \bar{\psi}_{\text{bt},0} + \beta y)|_{(x_c, y_c)} = \frac{\alpha \pi^2}{r^2} \sqrt{1 - \frac{\beta r}{\alpha \pi}}$$

$$= \frac{\alpha \pi^2}{r^2} \sqrt{1 - \frac{\alpha_c}{\alpha}} = \frac{\alpha \pi^2}{r^2} \sqrt{x_r}. \tag{56}$$

The period of the lower recirculating mode can, thus, be approximated as

$$T_{1,1} \lesssim \frac{2r^2}{\alpha \pi \sqrt{1 - \alpha_c/\alpha}} = \frac{2r^2}{\alpha \pi \sqrt{x_r}}. \tag{57}$$

At least for sufficiently weak forcing, their frequencies thus lie outside the range of Rossby basin modes and are smaller than the smallest basin-mode frequency. A stronger forcing elevates the frequency of recirculating modes. The spectra of basin and recirculating modes may overlap: the resulting modes exhibit a signal both in the recirculation gyre and in the eastern part of the basin. Figure 9 illustrates these modes in the double-gyre case.

For the lowest friction achieved (a higher resolution would have enabled us to use a lower friction, but requires unrealistic computer resources), the recirculating modes are restricted to the closed contour pool and their influence in the basin interior is very limited (vice versa the deformed Rossby basin modes have very little influence in the pool interior). However, increase of the friction coefficient causes leaking of the recirculating modes into the basin interior through a first lobe across the pool frontier (Fig. 10); at the highest friction used, a second, but opposite, lobe even occurs. Conversely the deformed basin modes leak into the interior of the pool until the frictional boundary layer grows across the

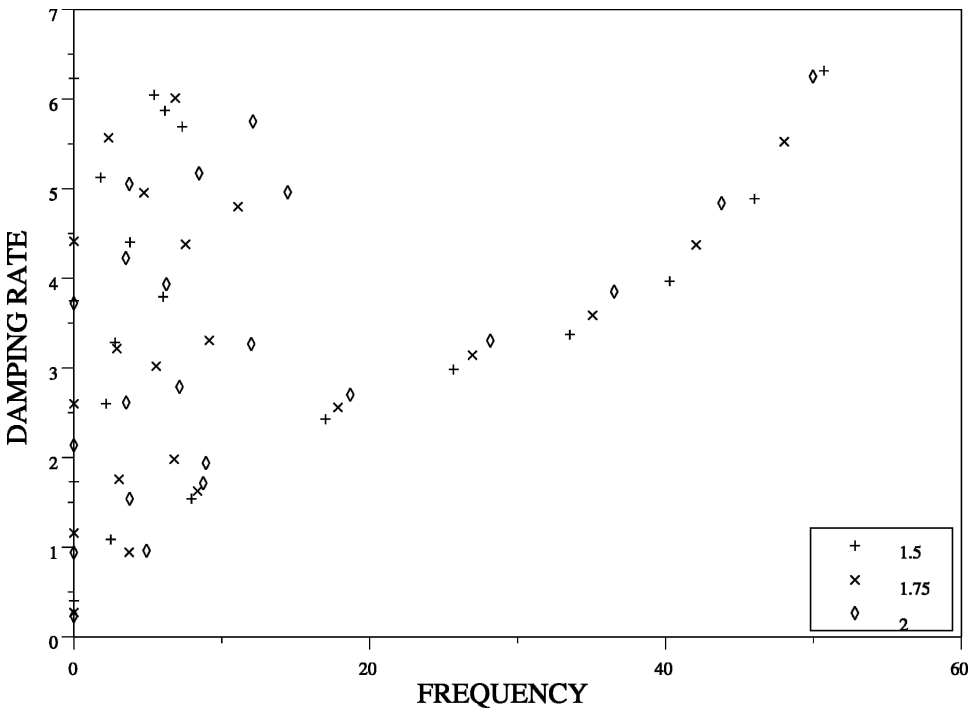

FIG. 6. Modes, frequency, and damping rate for increasing strength of the barotropic gyre ($\alpha/\alpha_c > 1$) corresponding to closed geostrophic contours. Note the emergence of numerous low-frequency modes missing at lower values of α (Fig. 2).

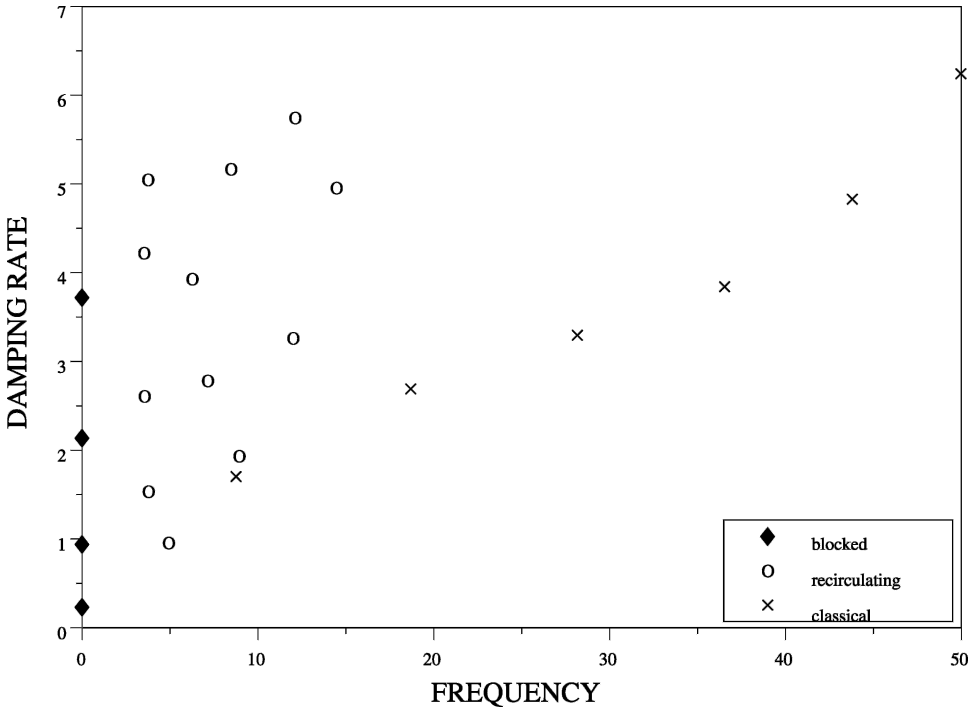

FIG. 7. Eigenvalues for classical Rossby, recirculating, and stationary blocked modes ($\alpha/\alpha_c = 2$).

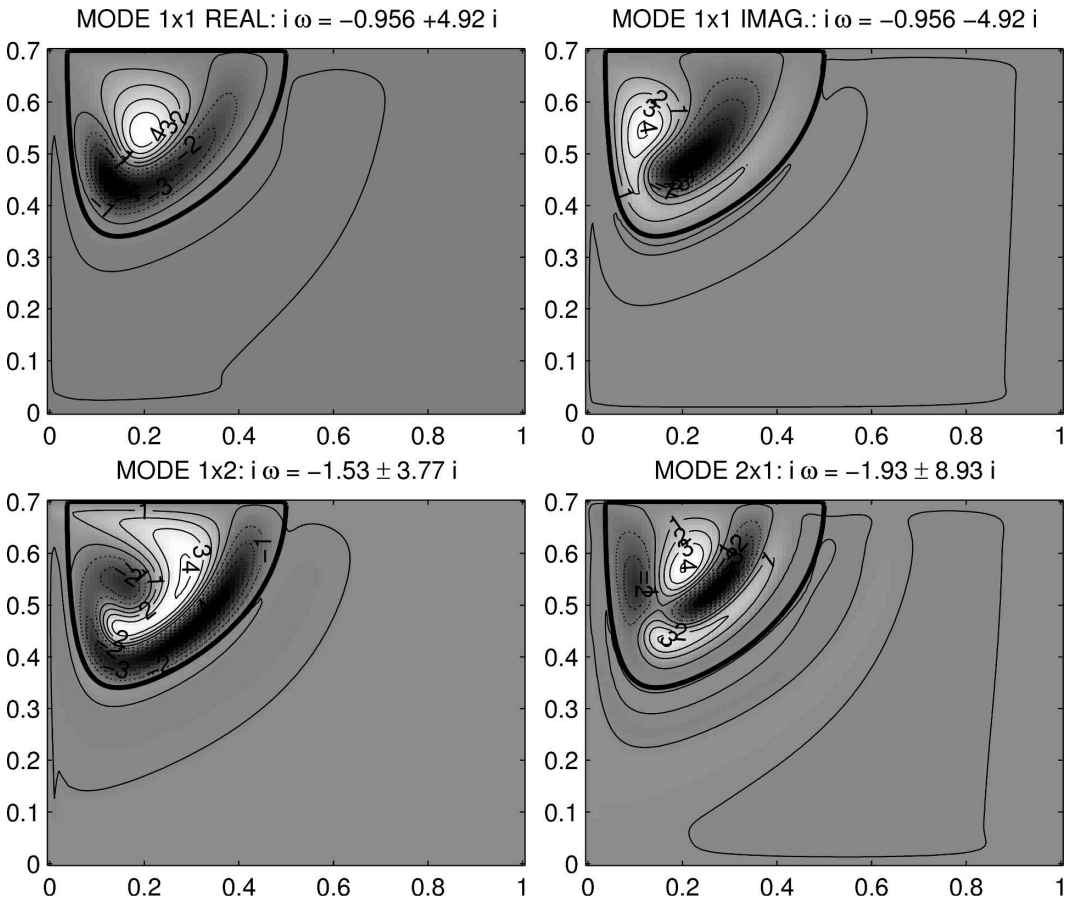

FIG. 8. The least damped low-frequency recirculating modes patterns for $\alpha/\alpha_c = 2$. Real and imaginary parts of mode 1×1 are provided to show the clockwise propagation in the closed geostrophic contours pool, but only one phase of models 1×2 and 2×1. Axes are longitude and latitude in nondimensional units.

whole pool. Figure 11 highlights the same behavior when the Burger number is increased for a fixed friction coefficient.

On the other hand, SC03 showed shadow modes and oscillatory pool modes both significantly leaking in the opposite region. This is not surprising given the limits of their numerical method with respect to the resolution across the separatrix (as discussed previously) where the smallest scales precisely develop.

Last, the mass-conserving boundary condition has little influence on the damping rate of these modes in contrast with the deformed Rossby basin modes (Cessi and Primeau 2001): their signature is very small on the (western part of the northern) boundary, as well as on the separatrix and rest of the basin outside the pool.

c. Stationary pool modes

In addition to the oscillatory modes, stationary modes do exist under the same conditions as above. They realize an exact local balance between mean-flow eastward advection, Rossby wave westward propagation, and diffusion; this can only hold within the closed-contour pool. In the inviscid limit they satisfy

$$J(\phi_i, \overline{\psi}_{\mathrm{bt},0} + \beta y) = 0. \tag{58}$$

Thus, a family of real valued functions $\{f_i\}_{i \in \mathbb{N}}$ exists such that

$$\phi_i = f_i(\overline{\psi}_{\mathrm{bt},0} + \beta y), \quad i \in \mathbb{N}. \tag{59}$$

Even though these modes have no equivalent in the closed basin because of the vanishing zonal velocity on the meridional boundaries, they are the analog of the stationary zonal flow solution in a zonal periodic canal: in both cases their streamfunctions are function of potential vorticity only. They can be seen as oscillating pool modes with a zero azimuthal wavenumber.

Figure 12 illustrates the large-scale least-damped stationary modes, indexed by their number of maxima, when $\alpha = 2\alpha_c$.

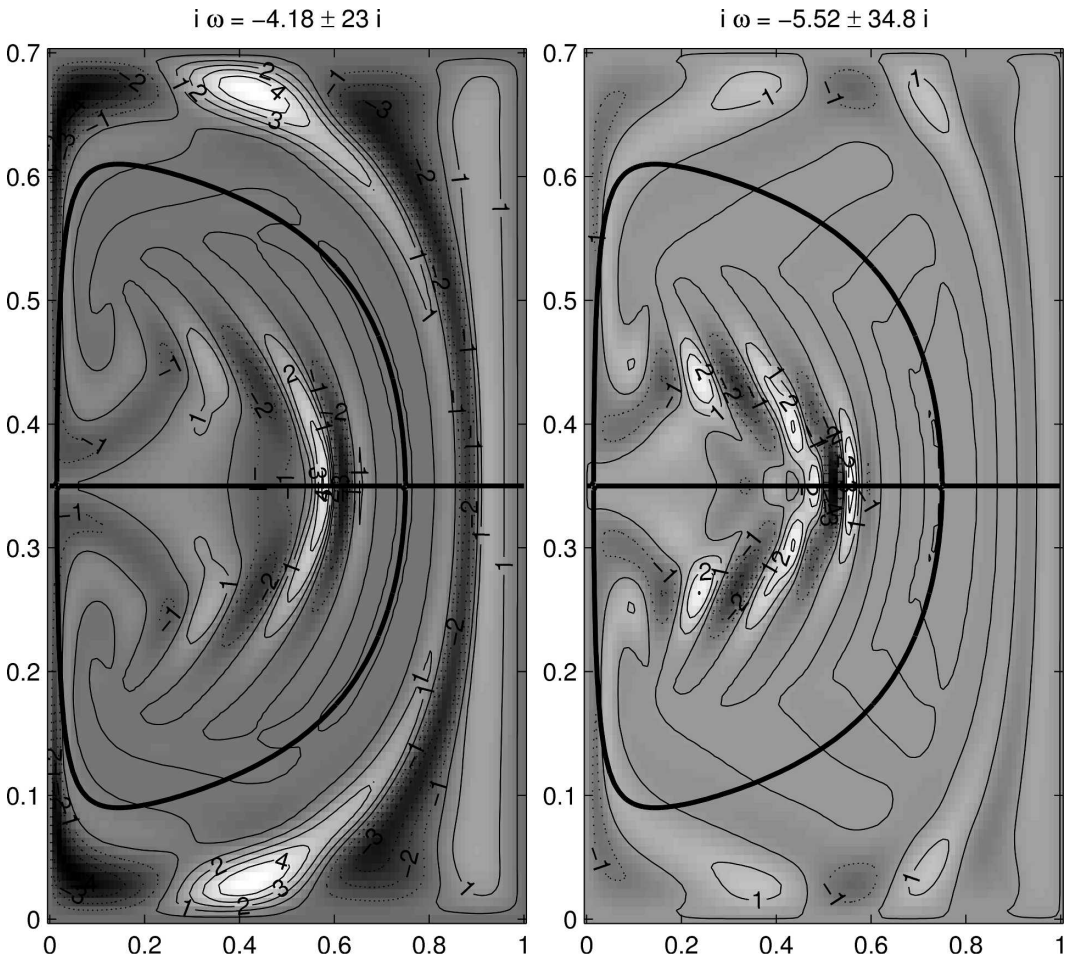

FIG. 9. Two mixed recirculating/classical Rossby modes patterns for $\alpha/\alpha_c = 4$ in the double-gyre case. Only one phase of each mode is shown. Axes are longitude and latitude in nondimensional units.

The stationary pool modes form a base for the operator $\mathcal{Q}^{-1}\mathcal{T}$ kernel. Each stationary pool mode (ϕ_i) is associated with a function (f_i) of potential vorticity only. These functions are a reminiscence of the degeneracy of the forced solution (39) where the function f is undetermined. Equation (51) shows they provide a natural base for decomposing the function $f = \Sigma_{i\in\mathbb{N}} 2B_0(0, i; t_2)f_i$.

In the inviscid limit, these modes are not damped (on time t_1), and we expect their amplitude evolution (on time t_2) to result from the higher-order dynamics (i.e., including baroclinic instability and dissipation). It would then be interesting to compute their equilibrium amplitude and compare it with the solution by Young and Rhines (1982).

By varying dissipation, Spydell and Cessi (2003) suggested a potential connection between the deformed basin modes (their shadow modes) and the stationary pool modes: in the inviscid limit, the qualitative change of the geostrophic contours topology may better explain the emergence of these modes.

6. Discussion and conclusions

We studied the quasigeostrophic baroclinic mode evolution equation in the presence of a steady barotropic flow by using an asymptotic analysis with the Burger number as small parameter. We demonstrated that the modes are neutral at the first order of the expansion (in the inviscid case) and underlined the role of dispersive terms to satisfy the boundary conditions. In contrast with previous studies, this was obtained through a well-posed problem requiring no dissipation parameterization at this order of the expansion. We then solved the equation numerically (with some necessary dissipation, at least for realistically small Burger number) and identified three types of low-frequency, large-scale modes: the classical Rossby basin modes deformed by the mean

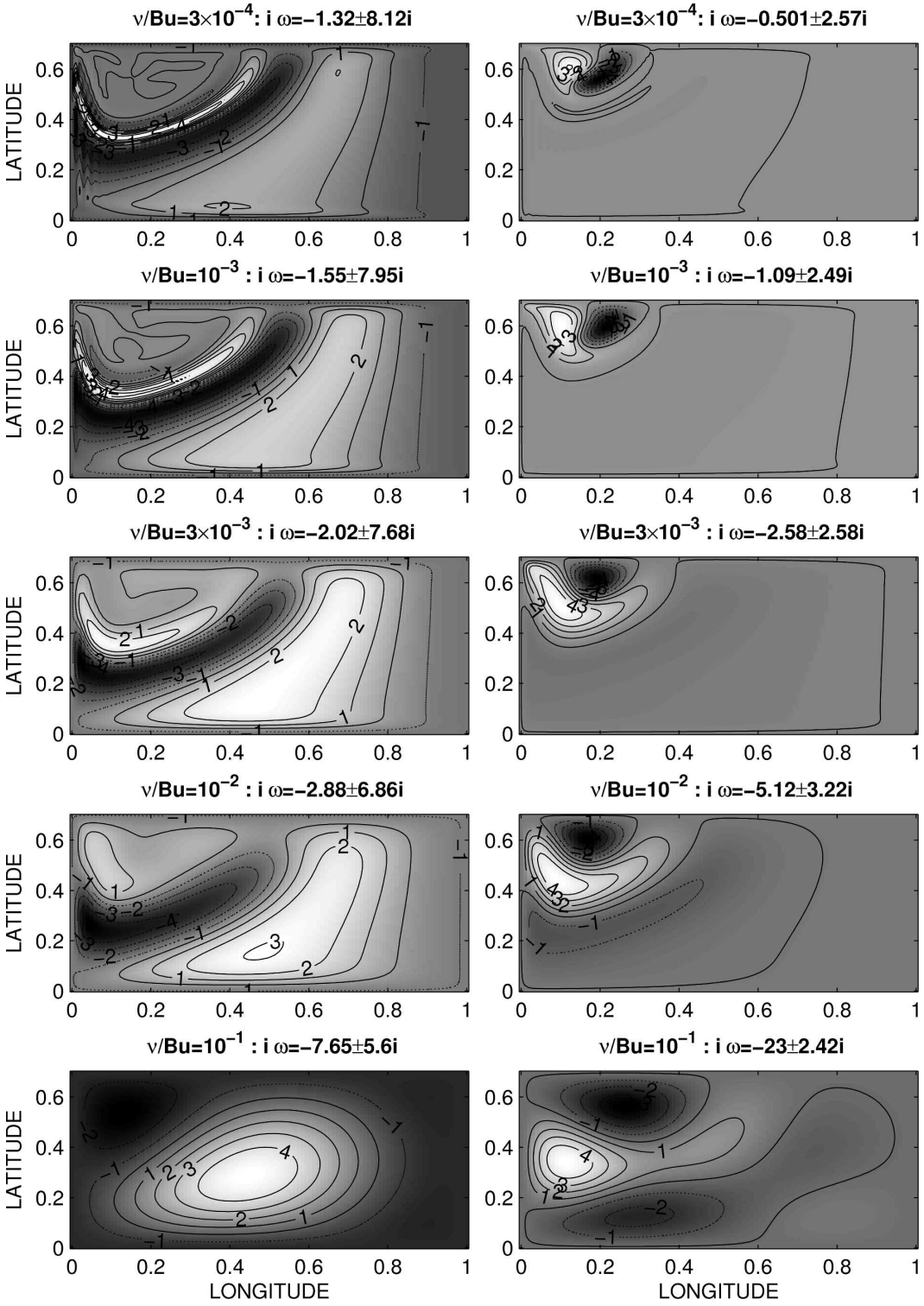

FIG. 10. Deformed Rossby basin modes and recirculating pool modes as a function of the friction coefficient (α/α_c = 1.5). Only one phase of each oscillatory mode is shown. Zero contour is not labeled. Note the leaking of each mode into the opposite region with increasing friction.

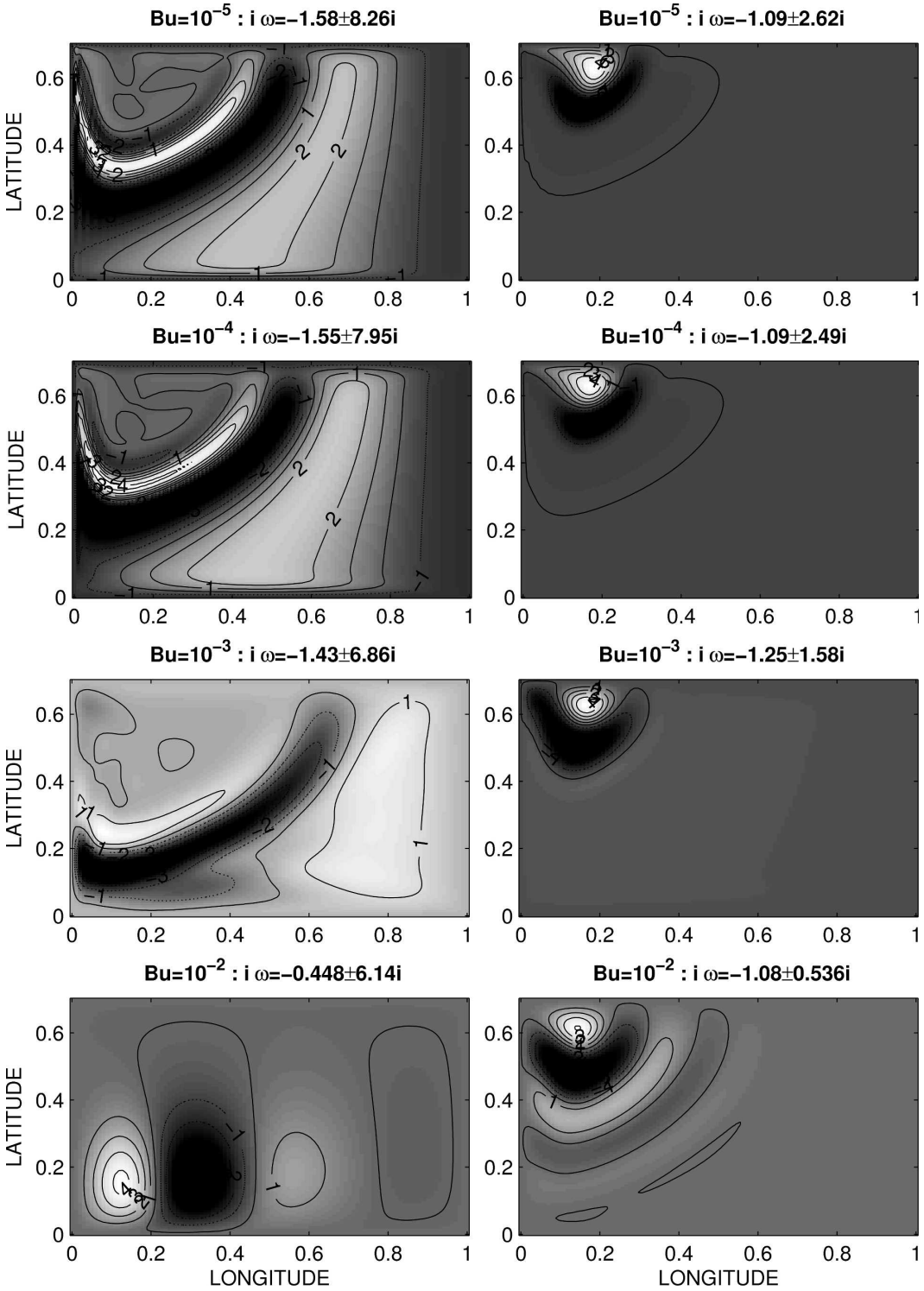

FIG. 11. Deformed Rossby basin modes and recirculating pool modes as a function of the Burger number ($\alpha/\alpha_c = 1.5$). Only one phase of each oscillatory mode is shown. Zero contour is not labeled. Note the leaking of each mode into the opposite region with increasing Burger number.

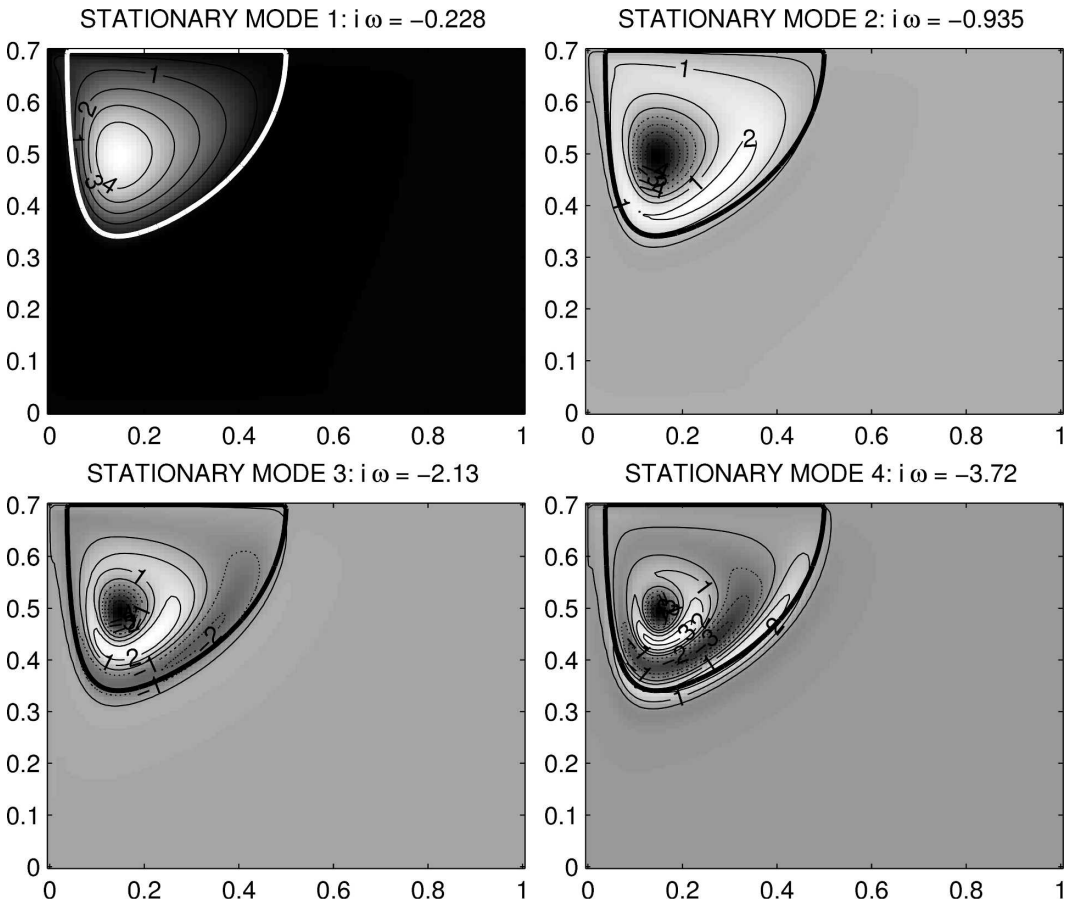

FIG. 12. Stationary blocked modes in the recirculating gyre ($\alpha/\alpha_c = 2$). The thick contour line indicates the limit of the closed geostrophic contours pool. Axes are longitude and latitude in nondimensional units.

flow (shadow modes in SC03), and stationary and recirculating pool modes depending on the existence of a recirculating pool where baroclinic waves are arrested by the mean flow. Under strong enough forcing, recirculating pool modes could resonate with the Rossby basin modes.

In the inviscid limit, the different oscillating modes can be seen as the result of coupling of the classical basin modes with different meridional wavenumbers by the barotropic advection. By continuously increasing its intensity, the spectrum of the modes is continuously modified. Further to a qualitative change in the geostrophic contours topology through the occurrence of closed geostrophic contours, northwestern intensified modes become recirculating pool modes, and the stationary pool modes arise as a new class of modes. We may conjecture that the necessarily continuous evolution of the modes spectrum would allow new modes to appear only on its edge, that is, at zero frequency.

In our numerical solutions, dissipation scales remain larger than the dispersive scale (Rossby radius of deformation) and friction controls the modes damping rate, in contrast with SC03. If we could reduce the dissipation scale to actually resolve the deformation radius, we would expect the small-scale, low-frequency Rossby waves to appear in the mode solution (and allow the boundary condition to be satisfied even in the inviscid limit). Indeed, we verified it by increasing the Rossby radius of deformation ($\mathrm{Bu} = 10^{-2}$) and found the resulting inviscid eigenmodes to be actually neutral.

Moreover, the oscillating trapped modes achieve the lowest frequency (and damping rate) for moderate recirculating gyre(s). They propagate along closed geostrophic contours, like the basin Rossby modes on constant potential vorticity contours, with no need of reinitiation of baroclinic waves from the western to the eastern boundary through rapid mass adjustment processes. Their frequency is, thus, rationalized through westward Rossby wave propagation (β effect) dominating in the southern half of the pool and eastward advection by the barotropic flow dominating in the northern half. For the lowest friction used, these modes have

no signature outside the pool, but their structure leaks into the basin interior when the friction coefficient or the Burger number is increased.

Although the model used here considers two layers spanning the whole water depth, a more appropriate setting would be to consider two active layers on top of a resting abyss. Values of α/α_c suggest, here, very limited recirculating gyres, whereas pools of homogenized potential vorticity are expected in the ocean. Such a reduced-gravity, two-layer model is now under investigation.

These basin modes are possible vectors of interannual variability. White noise atmospheric forcing is a candidate for exciting these large-scale weak damped modes (Cessi and Primeau 2001), but they could also arise from instability of the mean flow resulting from a stationary wind forcing (Dijkstra 2000). Under a strong enough wind forcing, Nauw and Dijkstra (2001) showed the emergence of a low-frequency, unstable baroclinic gyre mode very similar to the recirculating pool mode exposed here. Direct extension of the present study could provide an analytical framework to such instabilities by proceeding to the next order of the expansion, like in the barotropic case (Ben Jelloul and Huck 2003). Indeed, at the order considered here, the energy is mainly potential and conserved, which prevents the development of baroclinic instability. Proceeding to the next order should provide amplitude equations for every mode and analytical expressions for their growth rate. Stability criteria could then be derived for both stationary and oscillatory modes.

Unstable modes can be fed by meridional baroclinic shear of the mean flow (Pedlosky 2002) or induce potentially unstable meridional currents. The advecting role of the barotropic mean flow, like the latitude variation of the β parameter (J. H. LaCasce and J. Pedlosky 2003, personal communication), accelerates the wave front and thus produces a more zonal structure in the southern part of the basin. This may have a stabilizing effect in agreement with the observations of a long Rossby waves signature mainly south of the subtropical gyre (Chelton and Schlax 1996). On the other hand, LaCasce and Pedlosky (2004) showed that slow basin modes are baroclinically unstable and may have great difficulty crossing the basin in midlatitudes, which limits their coherent propagation to tropical regions.

However, the wind-driven circulation is better represented in a reduced-gravity, two-layer model than the one used here: Baroclinic instability through potential energy transfer from the stationary flow to the eventually unstable modes would then be more important, whether this feeds the baroclinic basin modes and allow them to grow (Colin de Verdière and Huck 1999) or destabilizes them into smaller scales. This is left for future investigations.

Acknowledgments. Computational facilities were provided by the Institut du Développement et des Ressources en Informatique Scientifique (IDRIS, Orsay, France). We thank J. Pedlosky and A. Colin de Verdière for comments on an earlier draft of the manuscript and L. Marié for his help with the numerics of large sparse matrices eigenanalysis. Thanks to the thorough and demanding comments of two anonymous reviewers, we supplemented the paper with new results initially thought to be unreachable and, we hope, clarified the presentation and interpretation. MBJ was supported by the Ocean and Climate Change Institute, Woods Hole Oceanographic Institution, during part of this work.

REFERENCES

Ben Jelloul, M., and T. Huck, 2003: Basin-mode interactions and selection by the mean flow in a reduced-gravity quasigeostrophic model. *J. Phys. Oceanogr.,* **33,** 2320–2332.

Cessi, P., and S. Louazel, 2001: Decadal oscillation response to stochastic wind forcing. *J. Phys. Oceanogr.,* **31,** 3020–3029.

——, and F. Primeau, 2001: Dissipative selection of low-frequency modes in a reduced-gravity basin. *J. Phys. Oceanogr.,* **31,** 127–137.

Chelton, D. B., and M. G. Schlax, 1996: Global observations of oceanic Rossby waves. *Science,* **272,** 234–238.

Colin de Verdière, A., and T. Huck, 1999: Baroclinic instability: An oceanic wavemaker for interdecadal variability. *J. Phys. Oceanogr.,* **29,** 893–910.

Delworth, T. L., and R. J. Greatbatch, 2000: Multidecadal thermohaline circulation variability driven by atmospheric surface flux forcing. *J. Climate,* **12,** 1481–1495.

——, S. Manabe, and R. J. Stouffer, 1993: Interdecadal variations of the thermohaline circulation in a coupled ocean–atmosphere model. *J. Climate,* **6,** 1993–2011.

Dewar, W. K., and R. X. Huang, 2001: Adjustment of the ventilated thermocline. *J. Phys. Oceanogr.,* **31,** 1676–1696.

Dijkstra, H. A., 2000: *Nonlinear Physical Oceanography: A Dynamical Systems Approach to the Large-Scale Ocean Circulation and El Niño.* Vol. 22, Kluwer Academic, 480 pp.

Flierl, G. R., 1977: Simple application of McWillimas "A note on a consistent quasi-geostrophic model in a multiply connected domain." *Dyn. Atmos. Oceans,* **1,** 443–453.

Greatbatch, R. J., and S. Zhang, 1995: An interdecadal oscillation in a idealized ocean basin forced by constant heat fluxes. *J. Climate,* **8,** 81–91.

Kushnir, Y., 1994: Interdecadal variations in North Atlantic sea surface temperature and associated atmospheric conditions. *J. Climate,* **7,** 141–157.

LaCasce, J. H., 2000: Baroclinic Rossby waves in a square basin. *J. Phys. Oceanogr.,* **30,** 3161–3178.

——, and J. Pedlosky, 2002: Baroclinic Rossby waves in irregular basins. *J. Phys. Oceanogr.,* **32,** 2828–2847.

——, and ——, 2004: The instability of Rossby basin modes and the oceanic eddy field. *J. Phys. Oceanogr.,* **34,** 2027–2041.

Larichev, V. D., 1974: Statement of an internal boundary-value problem for the Rossby-wave equation. *Izv. Atmos. Ocean. Phys.,* **10,** 470–473.

Lehouck, R. B., D. C. Sorensen, and C. Yang, 1998: *ARPACK Users' Guide: Solution of Large-Scale Eigenvalue Problems with Implicitly Restarted Arnoldi Methods*. SIAM, 160 pp. [Available online at http://www.caam.rice.edu/software/ARPACK/.]

Longuet-Higgins, M. S., 1964: Planetary waves on a rotating sphere. *Proc. Roy. Soc. London,* **279A,** 446–473.

Mann, M. E., R. S. Bradley, and M. K. Hughes, 1998: Global-scale temperature patterns and climate forcing over the past six centuries. *Nature,* **392,** 779–787.

McWilliams, J. C., 1977: A note on a consistent quasigeostrophic model in a multiply connected domain. *Dyn. Atmos. Oceans,* **1,** 427–441.

Nauw, J. J., and H. A. Dijkstra, 2001: The origin of the low-frequency variability of double gyre wind-driven flows. *J. Mar. Res.,* **59,** 567–597.

Pedlosky, J., 1987: *Geophysical Fluid Dynamics.* 2d ed. Springer-Verlag, 710 pp.

——, 1996: *Ocean Circulation Theory.* Springer-Verlag, 460 pp.

——, 2002: The destabilization of Rossby normal modes by meridional baroclinic shear. *J. Phys. Oceanogr.,* **32,** 2418–2423.

Primeau, F., 2002: Long Rossby wave basin-crossing time and the resonance of low-frequency basin modes. *J. Phys. Oceanogr.,* **32,** 2652–2665.

Sirven, J., and C. Frankignoul, 2000: Variability of the thermocline due to a sudden change in the Ekman pumping. *J. Phys. Oceanogr.,* **30,** 1776–1789.

Spydell, M., and P. Cessi, 2003: Baroclinic modes in a two-layer basin. *J. Phys. Oceanogr.,* **33,** 610–622.

Young, W. R., and P. B. Rhines, 1982: A theory of the wind driven circulation. Part II: Gyres with western boundary layer. *J. Mar. Res.,* **40,** 849–872.